

Energy dissipation and the spectral distribution of whitecaps

Jim Thomson,¹ Johannes R. Gemmrich,² and Andrew T. Jessup¹

Received 15 March 2009; revised 19 April 2009; accepted 5 May 2009; published 3 June 2009.

[1] Energy dissipation by breaking water waves is quantified indirectly using remote observations (digital video recordings) and directly using in situ observations (acoustic Doppler velocity profiles). The analysis is the first validation using field data to test the Duncan-Phillips formulation relating energy dissipation to the spectral distribution of whitecap speeds and lengths. Energy dissipation estimates are in agreement over two orders of magnitude, and demonstrate a promising method for routine observation of wave breaking dynamics. Breaking statistics are partitioned into contributions from waves at the peak of the wave-height spectrum and waves at higher frequencies in the spectrum. Peak waves are found to be only 10% of the total breaking rate, however peak waves contribute up to 75% of the total dissipation rate. In addition, breaking statistics are found to depend on the peak wave steepness and the energy input by the wind. **Citation:** Thomson, J., J. R. Gemmrich, and A. T. Jessup (2009), Energy dissipation and the spectral distribution of whitecaps, *Geophys. Res. Lett.*, *36*, L11601, doi:10.1029/2009GL038201.

1. Introduction

[2] The breaking of ocean surface waves is an important mechanism for air-sea interaction and for controlling wave growth, yet field quantification of breaking is limited [Banner and Peregrine, 1993; Melville, 1996]. Lack of breaking quantification thus limits global air-sea exchange estimates and operational wave predictions [Jensen *et al.*, 2002]. Remote sensing is a promising approach to fill this data gap, but the extent to which remote signals can be related to dynamic quantities remains largely unknown. Here we use field observations to successfully validate a relationship between the distribution of breaking waves and the energy dissipation rate, and then examine the scale dependence of the breaking activity.

[3] Phillips [1985] introduced $\Lambda(c)$, the distribution of total breaking crest lengths per unit area in bands of speed $c + dc$, defined by

$$L_{\text{total}} \equiv \int \Lambda(c)dc, \quad (1)$$

where L_{total} is the average total length of breaking crests per unit area. The distribution is useful as a spectral description of wave-breaking kinematics, with potential extension to

wave-breaking dynamics. In particular, the first moment of $\Lambda(c)$ is directly equivalent to the breaking rate at a point,

$$R_{\Lambda} = \int c\Lambda(c)dc. \quad (2)$$

Higher moments of $\Lambda(c)$ are indirectly related to the dynamics. Since energy dissipation is proportional to c^5 [Duncan, 1981], Phillips [1985] hypothesized that the total energy dissipation rate would be

$$E_{\Lambda} = \frac{b\rho_w}{g} \int c^5\Lambda(c)dc, \quad (3)$$

where g is gravity, ρ_w is the density of water, and b is a numerical constant predicted to be small. This so-called “breaking parameter” b is necessary to complete the conceptual model of a breaking crest extracting a fraction of the available wave energy by exerting a stress on the front face of the wave (and against the background orbital motion). As detailed by Gemmrich *et al.* [2008], the breaking parameter b thus incorporates the wave slope, the density anomaly of the foam, the ratio of crest to wavelength, and the ratio of orbital velocity to phase speed.

[4] Practical application of $\Lambda(c)$ observations requires in situ measurements of the dissipation rate to validate equation (3) and estimate the breaking parameter b , but such in situ measurements have been missing from previous $\Lambda(c)$ studies [Gemmrich *et al.*, 2008; Melville and Matusov, 2002; Phillips *et al.*, 2001]. Rather, previous studies have compared E_{Λ} with the energy input by the wind [Gemmrich *et al.*, 1994; Terray *et al.*, 1996], assuming a local equilibrium between the wind input and the dissipation due to breaking. Published values for b vary from $O(10^{-4})$ [Gemmrich *et al.*, 2008] to $O(10^{-2})$ [Melville and Matusov, 2002]. Recent work by Drazen *et al.* [2008] reviews these values, as well as laboratory estimates, and incorporates new data to suggest that b is of order $(2ak)^{5/2}$, where ak is the wave steepness given by the wave amplitude a and wave-number k .

2. Field Observations

[5] Digital video recordings and acoustic Doppler velocity profiles of breaking surface waves were collected during two field experiments on board the *R/V Henderson* (APL-UW). The sites were selected to have deep-water, fetch-limited conditions for local wind waves (i.e., wind chop), and to neglect larger scale motions (e.g., swell, tides, currents). In November 2006, the *Henderson* was stationed at the north end of Lake Washington, WA, USA (N 47°44.542', W 122°16.518') in 12-m water depth. In February 2008, the *Henderson* was stationed on Puget

¹Applied Physics Laboratory, University of Washington, Seattle, Washington, USA.

²Department of Physics and Astronomy, University of Victoria, Victoria, British Columbia, Canada.

Sound near Richmond Beach, WA, USA (N 47°46.795', W 122°23.950') in 19-m water depth.

[6] The video camera (Pt Grey Research *Flea*, Vancouver, BC) was deployed from a tower 10 m above the surface at a 50° incidence angle. The acoustic Doppler velocity profilers (SonTek *Dopbeam*) were deployed from a boom 1 m below the surface and cantilevered out 8.7 m meters away from the vessel. The *Henderson* has a catamaran hull design, and the instruments were deployed along the line between the hulls (2.4 m separation) to minimize interference by wave reflection from the hulls. The field-of-view from the video camera was approximately 20 m by 20 m, centered on the Dopbeam boom, and the mid-field pixel resolution was approximately 1 cm. The Dopbeams were aligned to collect vertical and horizontal profiles of water velocity, with bin resolutions of 0.6 cm. All instruments were sampled at 20 Hz.

[7] Each experiment included observations of a wind event lasting several hours, beginning with calm conditions and building to maximum sustained winds of 15 m s⁻¹, as measured by an ultrasonic anemometer (R.M. Young, Traverse City, MI) at a height of 8 m above the water surface and corrected to the standard U_{10} [Edson et al., 1991]. Analysis is restricted to the strongest event from each experiment, during which southerly winds forced waves along the axis of Lake Washington and Puget Sound and the fetch distances were approximately 7 and 20 km, respectively. Results are presented using ten 30-minute averages from each experiment, covering the observed range of breaking conditions.

[8] The wave fields grew to amplitudes a of approximately 0.25 m during these events, as measured by an ultrasonic altimeter (Siemens Milltronics *AiRanger DPL*, New York, NY). Wave height spectra, shown by J. Gemmrich (Strong turbulence in the wave crest region, submitted to Journal of Physical Oceanography, 2009), have a clear f^{-4} equilibrium shape [Banner, 1990], where f is frequency, and the peak frequency f_p varies from 0.56 to 0.33 Hz. The wavenumber k_p and phase speed c_p at the peak frequency band is calculated from the deep-water dispersion relation. The values are used to estimate wave steepness as ak_p , which varies from 0.03 to 0.12, and wave age as c_p/U_{10} , which varies from 0.3 to 0.6.

3. Methods

[9] Methods used to process the data are described in detail by Thomson and Jessup [2009] and Gemmrich (submitted manuscript, 2009) for the video recording and velocity profiles, respectively. The methods are reviewed here briefly for completeness.

3.1. Remote Methods

[10] Video data are rectified and then processed using a difference-threshold to identify the leading edge of each breaking crest. The resulting binary record $I(x,y,t)$ is then Fast Fourier Transformed to a frequency-wavenumber spectrum $S(k_x, k_y, f)$, which is mapped to a speed spectrum $S(c)$ using the change of variable $c = f/k$ [Chickadel et al., 2003]. Finally, the speed spectrum is renormalized to obtain [Thomson and Jessup, 2009]

$$\Lambda(c) = S(c) \cdot \frac{dx \sum I(x,y,t)}{NA \int S(c)dc}, \quad (4)$$

where N is the number of images, A is the rectified image area, and dx is the along-crest pixel size.

[11] This method has been validated using equivalent time-domain methods, and by comparing the breaking rate given by the first moment of the distribution, R_Λ (equation (2)), to the breaking rate obtained via direct counting at all $M \times N$ video pixels

$$R_D = \frac{\sum \sum \sum I(x,y,t)}{M \cdot N \cdot dt}. \quad (5)$$

The agreement is documented by Thomson and Jessup [2009] and is shown in Figure 1a. For dynamic quantities, the observed speeds c must be corrected to the associated phase speeds using the empirical result that breaking crests travel at approximately 80% of the related (nonbreaking) phase speed [Gemmrich et al., 2008; Melville and Matusov, 2002; Phillips et al., 2001]. This introduces a correction factor of $(0.8)^5$ in equation (3).

3.2. In Situ Methods

[12] Acoustic Doppler velocity profiles are processed to estimate the vertical structure function $D(z,r)$ of water velocity fluctuations, after removal of wave orbital motions, where z is the vertical location and r is the distance between velocity fluctuations [Wiles et al., 2006]. Assuming a cascade of isotropic eddies in the inertial subrange, $D(z,r)$ has the form $Ar^{2/3}$ and the total energy dissipation rate is given by Gemmrich (submitted manuscript, 2009)

$$E_D = \rho_w \int \left(\frac{C_v^2}{A} \right)^{3/2} dz, \quad (6)$$

where C_v^2 is a constant, A is determined for each z , and the profiles are vertically integrated from $z = -0.5$ m up to the instantaneous surface level. The profiles of dissipation rate are dominated by the crest region, and thus ignoring dissipation more than 0.5 m below the surface has a negligible effect.

[13] Prior to comparison with the remote estimates, a constant background dissipation of 0.5 W m⁻² is removed from E_D . This background level is determined as the average dissipation observed during a 30-minute period where $\Lambda(c) = 0$ at all c (i.e., in the absence of visible breaking). The same background dissipation is observed for Lake Washington and Puget Sound, and the level is confirmed to be constant by using short (order 1 minute) non-breaking periods covering the range of conditions.

[14] Energy input from the wind is estimated using the wind stress $\tau = \rho_a u_*^2$, where ρ_a is the density of air and u_* is the air-side friction velocity determined from the inertial dissipation method [Edson et al., 1991]. The rate of energy input to the waves is estimated as a continuous stress acting on a surface moving at an effective speed c_e , such that [Gemmrich et al., 1994; Terray et al., 1996]

$$E_W = \rho_a c_e u_*^2, \quad (7)$$

where the phase speed of the peak waves c_p is used for c_e . This is in contrast to unlimited fetch conditions, where $c_e \ll c_p$, because the fetch-limited waves in Lake Washington

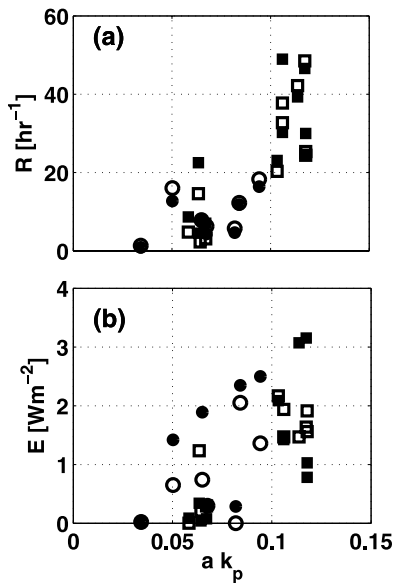


Figure 1. (a) Breaking and (b) energy dissipation rates as function of peak wave steepness. Data from Lake Washington (squares) and Puget Sound (circles) are shown together, with filled symbols showing the estimates from $\Lambda(c)$ (equations (2) and (3)) and open symbols showing direct estimates (equations (5) and (6)).

and Puget Sound are limited to the smaller scales where the wind stress acts (Gemrich, submitted manuscript, 2009).

4. Results

[15] Rates of breaking and of energy dissipation are shown in Figure 1 to be a strong function of wave steepness, consistent with previous field observations [Banner *et al.*, 2000]. There is considerable scatter in the energy dissipation rate compared with the breaking rate, suggesting a scale-dependent relationship more complicated than can be described using bulk statistics.

4.1. Scale Dependence

[16] The $\Lambda(c)$ distributions are shown in Figure 2 (dimensional, linear scale) and Figure 3 (normalized, log scale). In each experiment, there is a clear maximum in $\Lambda(c)$ indicating a dominant scale for wave breaking. As breaking activity (and steepness) increases, the dominant scale shifts to larger speeds (Figure 2). However, when the distribution is normalized by c_p , the dominant scale collapses around $c/c_p \approx 0.4$ (Figure 3). Thus, breaking scales grow with the wave field and breaking is most prevalent at scales significantly less than the peak in the wave height spectrum. There is almost no breaking observed at speeds greater than the peak phase speed (Figure 3a).

[17] Integrating over the peak scales, $0.7 > c/c_p > 1.3$, the peak contribution to the breaking rate is less than 10% of the total, but the peak contribution to the indirect dissipation rate is up to 75% of the total (average over all records is 67%). Restated, the large-scale breaking waves dominate the indirect dissipation estimate, even though they are infrequent. This is directly related to the convex shape of $\Lambda(c)$, which is consistent with observations by Gemrich *et al.* [2008] and Jessup and Phadnis [2005]. In contrast, the

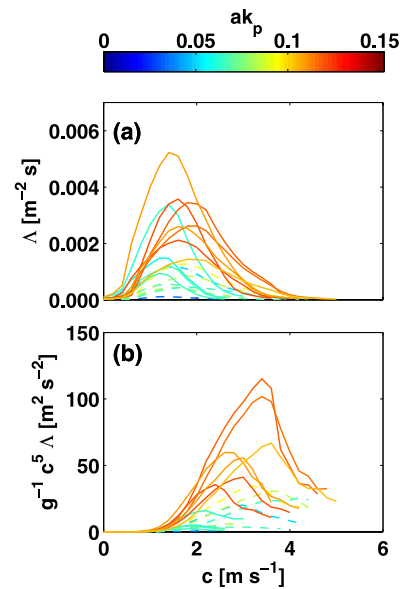


Figure 2. (a) Total breaking crest lengths and (b) unscaled energy dissipation as function of dimensional crest speed using a linear scale. Data from Lake Washington (solid lines) and Puget Sound (dashed lines) are shown together, and color indicates peak wave steepness.

descending c^{-6} shape of Melville and Matusov [2002] is only observed at the largest scales (Figure 3a).

4.2. Energy Dissipation Comparison

[18] The comparison of remote (indirect) and in situ (direct) energy dissipation estimates is shown in Figure 4a,

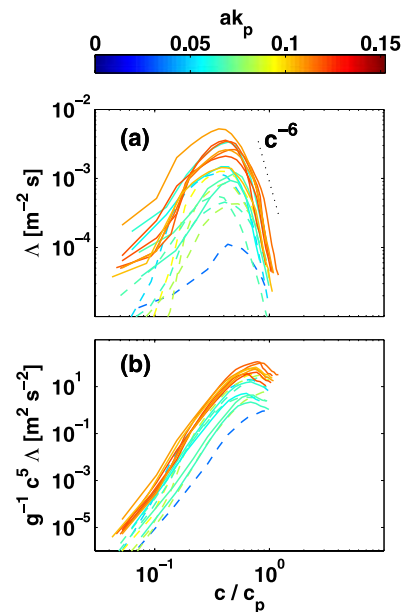


Figure 3. (a) Total breaking crest lengths and (b) unscaled energy dissipation as a function of non-dimensional speed (observed speed scaled by peak phase speed) using a logarithmic scale. Lines and colors as in Figure 2. The dotted line in Figure 3a indicates a c^{-6} dependence, which is approached near the phase speed of the peak waves.

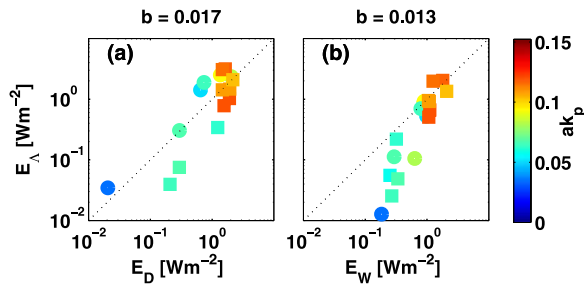


Figure 4. Total energy dissipation rates estimated from $\Lambda(c)$ compared with (a) in situ dissipation and (b) wind input. Data from Lake Washington (squares) and Puget Sound (circles) are shown together, and color indicates peak wave steepness. The difference in b values produces a slight shift in E_Λ from Figure 4a to Figure 4b.

and the comparison of remote (indirect) energy dissipation and wind forcing (indirect) is shown in Figure 4b. Both plots show good agreement over two orders of magnitude, with correlation values of $r = 0.7$ and $r = 0.8$, respectively. The wind comparison assumes equilibrium conditions, in which input balances dissipation, and that balance is clearly a poor assumption when waves are still growing (i.e., the mis-match for $ak_p < 0.1$ in Figure 4b).

[19] The direct estimate of the breaking parameter, obtained by comparison of E_Λ with E_D (equations (3) and (6)), is $b = 0.017 \pm 0.03$. The indirect estimate of the breaking parameter, obtained by comparison of E_Λ with E_W (equations (3) and (7)), is $b = 0.013 \pm 0.05$. Both are in the range of the recent $(2ak_p)^{5/2}$ empirical prediction by Drazen *et al.* [2008], as well as analytic predictions based on the stress [Duncan, 1981], the momentum [Phillips *et al.*, 2001], or the weight [Gemmrich *et al.*, 2008] of breaking crests. However, it is known that narrow fetches reduce wind input to waves [Atakturk and Katsaros, 1999], and thus these b estimates might not be applicable to oceanic conditions.

5. Conclusions

[20] The speed spectrum of breaking crest lengths, $\Lambda(c)$, is found to be a useful quantity for remote quantification of breaking wave kinematics and dynamics. In particular, rates of breaking and energy dissipation are consistent with direct observations. This validation is limited to narrow-fetch conditions, but extension to full oceanic conditions appears promising. These results can be applied to enhance routine observations of wave-breaking and to improve the dissipation term in predictive wave models.

[21] **Acknowledgments.** Thanks to field crews from APL-UW, including: D. Clark, E. Boget, A. deKlerk, C. Linder, R. McQuin, and P.J. Rusello. Thanks to M. Banner for insightful discussions during data processing. Facilities provided by Bill Evans at the Kenmore Parks Dept. and Brian Wuellner at Paramount Petroleum. Funding provided by the National Science Foundation (OCE 0549780) and the Office of Naval Research (N000140610809).

References

- Atakturk, S. S., and K. B. Katsaros (1999), Wind stress and surface waves observed on Lake Washington, *J. Phys. Oceanogr.*, *29*, 633–650.
- Banner, M. L. (1990), Equilibrium spectra of wind waves, *J. Phys. Oceanogr.*, *20*, 966–984.
- Banner, M. L., and D. H. Peregrine (1993), Wave breaking in deep water, *Annu. Rev. Fluid Mech.*, *25*, 373–397.
- Banner, M. L., A. V. Babanin, and I. Young (2000), Breaking probability for dominant waves on the sea surface, *J. Phys. Oceanogr.*, *30*, 3145–3160.
- Chickadel, C. C., R. A. Holman, and M. H. Freilich (2003), An optical technique for the measurement of longshore currents, *J. Geophys. Res.*, *108*(C11), 3364, doi:10.1029/2003JC001774.
- Drazen, D., W. K. Melville, and L. Lenain (2008), Inertial scaling of dissipation in unsteady breaking waves, *J. Fluid Mech.*, *611*, 307–332.
- Duncan, J. H. (1981), An experimental investigation of breaking waves produced by a towed hydrofoil, *Proc. R. Soc. London, Ser. A*, *377*, 331–348.
- Edson, J. B., C. W. Fairall, P. G. Mestayer, and S. E. Larsen (1991), A study of the inertial-dissipation method for computing air-sea fluxes, *J. Geophys. Res.*, *96*, 10,689–10,711.
- Gemmrich, J., T. Mudge, and V. Polonichko (1994), On the energy input from wind to surface waves, *J. Phys. Oceanogr.*, *24*, 2413–2417.
- Gemmrich, J. R., M. L. Banner, and C. Garrett (2008), Spectrally resolved energy dissipation rate and momentum flux of breaking waves, *J. Phys. Oceanogr.*, *38*, 1296–1312.
- Jensen, R., P. Wittmann, and J. Dykes (2002), Global and regional wave modeling activities, *Oceanography*, *15*, 57–66.
- Jessup, A., and K. Phadnis (2005), Measurement of the geometric and kinematic properties of microscale breaking waves from infrared imagery using a PIV algorithm, *Meas. Sci. Technol.*, *16*, 1961–1969.
- Melville, W. K. (1996), The role of surface-wave breaking in air-sea interaction, *Annu. Rev. Fluid Mech.*, *28*, 279–321.
- Melville, W. K., and P. Matusov (2002), Distribution of breaking waves at the ocean surface, *Nature*, *417*, 58–63.
- Phillips, O. M. (1985), Spectral and statistical properties of the equilibrium range in wind-generated gravity waves, *J. Fluid Mech.*, *156*, 495–531.
- Phillips, O. M., F. Posner, and J. Hansen (2001), High range resolution radar measurements of the speed distribution of breaking events in wind-generated ocean waves: Surface impulse and wave energy dissipation rates, *J. Phys. Oceanogr.*, *31*, 450–460.
- Terray, E., M. Donelan, Y. Agrawal, W. Drennan, K. Kahma, A. Williams, P. Hwang, and S. Kitaigorodskii (1996), Estimates of kinetic energy dissipation under breaking waves, *J. Phys. Oceanogr.*, *26*, 792–807.
- Thomson, J., and A. Jessup (2009), A fourier-based method for the distribution of breaking crests from video observations, *J. Atmos. Oceanic Technol.*, in press.
- Wiles, P. J., T. P. Rippeth, J. H. Simpson, and P. J. Hendricks (2006), A novel technique for measuring the rate of turbulent dissipation in the marine environment, *Geophys. Res. Lett.*, *33*, L21608, doi:10.1029/2006GL027050.

J. R. Gemmrich, Department of Physics and Astronomy, University of Victoria, Victoria, BC V8W 3P6, Canada. (jsgemmrich@uvic.ca)

A. T. Jessup and J. Thomson, Applied Physics Laboratory, University of Washington, 1013 NE 40th Street, Seattle, WA 98105, USA. (jessup@apl.washington.edu; jthomson@apl.washington.edu)